Surface & Coatings Technology 206 (2012) 2464–2473

Contents lists available at SciVerse ScienceDirect

Surface & Coatings Technology

journal homepage: www.elsevier.com/locate/surfcoat

Parametric study of suspension plasma spray processing parameters on coating microstructures manufactured from nanoscale yttria-stabilized zirconia

Kent VanEvery, Matthew John M. Krane, Rodney W. Trice *

School of Materials Engineering, Purdue University, United States

ARTICLE INFO

Article history:
Received 18 August 2011
Accepted in revised form 25 October 2011
Available online 4 November 2011

Keywords:
Suspension plasma spray
YSZ
Thermal barrier coating
TBC

ABSTRACT

A parametric study was conducted to determine the effect of suspension plasma spray (SPS) processing parameters, including plasma torch standoff, suspension injection velocity, injector location, powder loading in the suspension, and torch power, on the final microstructure of coatings fabricated from 80 nm diameter yttria-stabilized zirconia (YSZ) powders. Coatings made with different conditions were analyzed via stereology techniques for the amount of unmelted powder and spherical particles, which are undesirable features in a thermal barrier coating. Observation of unmelted powders, generally in the form of submicron-sized clusters of nanometer-sized powders, indicated insufficient plasma enthalpy or time in the plume to evaporate the liquid carrier in the fragmented droplet and melt the remaining powders. For coatings produced with a 4 cm standoff, a suspension injection velocity of 23 m/s, or a torch power of 21 kW, unmelted powders covered between 20 and 50% of the surface area. The presence of micron-sized spherical particulates was an indication of either partial powder melting or complete melting and re-solidification of a YSZ powder cluster prior to impact with the substrate. A 6 cm standoff, suspension injection velocity of 15 m/s, or 10 wt.% YSZ powder suspension each yielded coatings in which spherical particles comprised more than 8% of the coating surface area. The parametric study findings and the plasma-spray literature were employed to further modify the SPS experimental parameters to produce coatings that minimize unmelted powder and spherical particulates. The improved spray parameters for 80 nm diameter YSZ particles were found to be suspensions comprised of 8 wt.% YSZ powder, a 21 m/s suspension injection velocity (corresponding a ~50 ml/min volumetric flow), a 5 cm standoff, and a torch power of 50 kW. With these conditions less than 2% of the coating top surface area was covered by unmelted powder and spherical particulates.

1. Introduction

Thermal barrier coatings (TBCs) are widely used in gas turbines to insulate metallic components from the heat generated during engine operation [1]. These coatings are commonly yttria-stabilized zirconia (YSZ) layers applied via the air plasma spray (APS) process [1–3], in which a carrier gas introduces powder into a plasma that melts and transports these particles to the surface being coated. Adhesion in APS coatings is mainly due to the interaction of the *melted* powders of YSZ with the metallic substrate or previously deposited layers. Thus, the production of APS TBCs is typically designed to minimize the amount of coating feedstock powders depositing on the substrate in a solid or partially-solid state. Recently, the TBC industry has shown interest in producing these coatings using the suspension plasma spray [4] (SPS) process. SPS differs from APS primarily in that a liquid replaces the powder carrier gas. This change makes producing coatings from micron-sized and smaller feedstock powders feasible by solving the problems associated with injecting these particles via a carrier gas, particularly the premature agglomeration of the small particles; further details are published elsewhere [5–8].

In SPS, the formation of the coating begins with the break-up of the suspension stream by the plasma into micron-scale droplets composed of many nanometer-scale particles of the starting powder in the liquid carrier. Undesirable deposits can appear in the coating as the original powder, indicating no significant melting of the feedstock by the plasma, or as spherical-shaped particulates, which can be linked to incomplete melting or re-solidification of the YSZ in the plasma prior to impact with the substrate. For the case of incomplete evaporation of the liquid carrier while in the plume, the impacting droplet will appear on the surface as irregularly-shaped, submicron-sized clusters of nanometer-sized powders. Using an SEM, individual nanometer-sized powders can be resolved within these clusters, indicating no melting of the powder.

The origin of spherical particulates on the surface can occur by at least two formation mechanisms, in both of which the solvent is completely evaporated prior to reaching the substrate. In the first, YSZ

* Corresponding author. Tel.: +1 765 494 6405 (Office); fax: +1 765 494 1204.
E-mail address: rtrice@purdue.edu (R.W. Trice).

0257-8972/$ – see front matter
doi:10.1016/j.surfcoat.2011.10.051

powders in the original droplet have only partially melted prior to striking the substrate. Thus, the YSZ particulate has a solid core of partially melted powders, but a completely melted exterior. The solid core reduces or prevents the spreading of the semi-solid particle, producing microstructural features appearing as hemispheres or spheres, depending on the degree of deformation. The second spherical particulate formation mechanism occurs when the powder-containing droplet is completely melted, but then partially re-solidifies before contact with the substrate. In this case, the YSZ particulate resists deformation on impact because it is fully solid or has a semi-solid shell over a melted core. Note that both forms of spherical particulates are micron-sized because they represent the partially melted agglomeration of many nanometer-sized YSZ powders from the original fragmented droplet.

Porosity, which would be expected for coatings comprised of unmelted powders or partially-melted particulates, generally lowers the thermal conductivity of a TBC due to inefficient packing in these microstructures and the near zero thermal conductivity of air. However, adequate mechanical or chemical bonding must exist between the deposited microstructural features to achieve acceptable strength and erosion resistance. Experiences with unmelted powders or partially-melted particulates in the final coating can result in a powdery coating that can be removed easily by minimum abrasion. Thus, the presence of unmelted powders or partially-melted particulates is desired to be minimized.

Minimizing the amount of powder and spherical particulate deposition during SPS requires maximizing the time the powder resides in plasma above the YSZ feedstock melting temperature (~2700 °C), and ensuring that the plasma has enough enthalpy to evaporate the liquid carrier, melt the powder, and keep the YSZ molten in-flight. However, when using a direct current (DC) arc to ionize gas, which is the most popular method of generating the plasma, processing parameter changes are subject to stringent tradeoffs among these requirements [8]. For example, the enthalpy of the plume produced by a DC plasma torch can be increased by raising the electric current and volume of gas flowing into the torch [8]. Each of these changes will also elevate the speed of the resulting plasma, which decreases the time the feedstock particles spend in the plume before reaching the substrate [9]. Additionally, as the plasma velocity climbs, the powder particles, which for this work were injected normal to the plasma flow, are less likely to reach the central, hottest regions of the plume before deposition [8]. This difficulty can be surmounted by increasing the suspension injection momentum, but the simplest way of achieving this increase is to raise the injection velocity and/or the powder mass fraction in the suspension, both of which will require more plasma enthalpy to melt completely the YSZ in the plume [8]. Furthermore, the above SPS processing problems are also complicated because the average YSZ particle, even after some agglomeration in the plume, can be an order of magnitude or more smaller than that in APS [7,8]. These smaller YSZ agglomerates respond more rapidly to changes in plasma temperature and velocity, altering significantly the process parameters necessary to generate a SPS coating from those of an APS process with the same feedstock material [10]. Consequently, optimizing the deposition of fully molten particulates during SPS TBC production requires a set of experiments designed to evaluate the results of varying processing parameters affecting feedstock injection, plasma enthalpy, and the torch-substrate standoff distance.

The present work focuses on determining processing parameters that minimized undesirable deposits in coatings manufactured via SPS. As a result, the authors conducted a parametric study of the amount of unmelted powder and spherical particulates in YSZ coatings produced with various SPS processing conditions and used the findings to understand better the phenomena influencing the depositing YSZ state. Based upon the results of the parametric study and literature reports, the spray parameters were further modified to minimize undesirable microstructural features.

2. Experimental procedures

2.1. Basis for SPS processing parameter selection

Prior SPS research involving conditions reproducible in the current study were used to reduce the number and range of the parameters investigated here. For example, ethanol was used as a suspension solvent because calculations by Chen et al. [11] showed that the total heat required to vaporize ethanol is one-third that of water. Furthermore, Siegert [12] found the deposition efficiency (DE), the ratio of the coating mass to the powder mass sprayed toward the substrate, doubled when switching from a water-based YSZ suspension to an ethanol-based YSZ suspension. Even with an ethanol solvent, the YSZ content of an injected suspension can exceed the capacity of the plasma to melt the powder completely. Chen et al. observed unmelted powder particles in SPS coatings generated from suspensions containing 25 wt.% YSZ [11]. Likewise, Kassner showed the fraction of porosity corresponding to unmelted powder tended to increase with suspension powder loadings from 10 to 30 wt.% [13]. The presence of powder within coatings was also used, along with DE, by the studies of [10–12,14], and [15] to place the optimal standoff for SPS with YSZ suspensions between 4 and 6 cm.

When injecting the suspension normal to the plume, nozzles producing coherent streams are reported to improve powder entrainment in the plasma core (i.e. the central, hotter regions) above what can be achieved with atomizing nozzles [12]. However, Oberste Berghaus et al. found that coherent stream nozzles below 100 μm in diameter tended to clog frequently when spraying suspensions containing 5–15 wt.% powder with 30–70 nm diameter particles [10]. For an ethanol–YSZ suspension containing 5–12 wt.% powder injected through a 200 μm diameter coherent stream nozzle, Siegert [12] states that 20–28 m/s injection velocities caused the majority of the 300 nm median diameter powder to reach the plasma core; similar findings were obtained by Oberste Berghaus et al. [10]. For these injection results [10,12], the suspension nozzle was located external to the torch and inclined at an angle from 60 to 78° relative to the main plasma flow direction. In a separate study, Oberste Berghaus et al. [16] employed a setup wherein the suspension was injected into the plasma inside the torch. Compared to external injection, injecting within the torch body increases the dwell time of the powder in the plasma.

Based upon the SPS research cited above, the present study investigated the depositing YSZ state changes with the following experimental parameter ranges: standoff distance (4–6 cm), suspension injection velocity (15–23 m/s), injector location (external and internal to torch body), powder concentration (2–10 wt.%) in an ethanol solvent, and torch power (21–50 kW).

2.2. Suspension and coating production

All coatings were made from ZrO_2–8 wt.% Y_2O_3 powders suspended in ethanol containing 1 wt.% of dissolved phosphate ester to aid powder dispersion.[1] The ZrO_2–8 wt.% Y_2O_3 in the suspensions was a nanopowder feedstock synthesized by Inframat® Advanced Materials (Manchester, CT). Nanoparticle suspensions were formulated at powder concentrations of 2, 5, 8, and 10 wt.%. After formulation the suspensions were milled for 3 h on a rolling jar mill to break apart agglomerates and coat the particles in dispersant. The YSZ grinding media employed for this process were 9.5 mm diameter by 9.5 mm long cylinders. The particle size distributions of each suspension were measured following milling using a Beckman Coulter® (Fullerton, CA) LS 230 particle size analyzer. These measurements showed that each suspension had a number-based d_{50} of ~80 nm, and that

[1] Dissolved phosphate ester to aid powder dispersion.

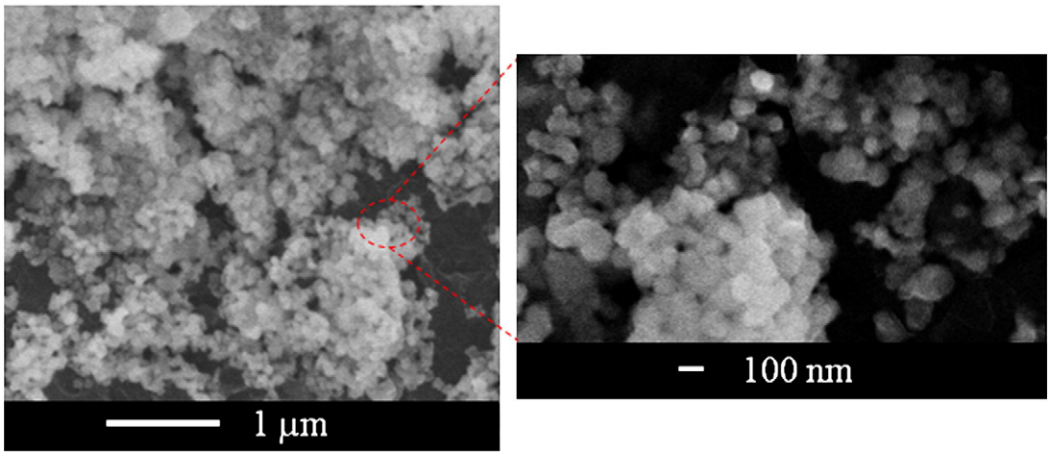

Fig. 1. SEM image of the starting YSZ powders prepared by placing a drop of suspension on a glass slide and allowing the ethanol to evaporate. Note the nanometer-sized features of the powders.

Table 1
Processing parameters used in the parametric study.

Experimental condition	Processing parameters						
	Injection velocity (m/s)	Suspension powder loading (wt.%)	Standoff distance (cm)	Ar/He gas mixture (slm)	Torch current (A)	Torch voltage (V)	Torch power (kW)
Baseline[a]	20	5	5	38/20	900	42	37.8
4 cm standoff[a]	20	5	4	38/20	900	42	37.8
6 cm standoff[a]	20	5	6	38/20	900	42	37.8
15 m/s injection velocity[a]	15	5	5	38/20	900	42	37.8
23 m/s injection velocity[a]	23	5	5	38/20	900	42	37.8
External injection[b]	20	5	5	38/20	900	42	37.8
2 wt.% powder loading[a]	20	2	5	38/20	900	42	37.8
10 wt.% powder loading[a]	20	10	5	38/20	900	42	37.8
Low plasma enthalpy[a]	20	5	5	46/0	600	35	21.0
High plasma enthalpy[a]	20	5	5	24/20	1200	35	42.0
Improved[a]	21	8	5	20/60	1000	50	50.0

[a] Suspension injected through a 230 μm dia. ruby orifice oriented orthogonal to the spray direction.
[b] Suspension injected through a 200 μm dia. stainless steel orifice at 75° angle to the spray direction.

no statistical difference existed between the median particle sizes of the different formulations. A density of 6.0 g/cm^3 and complex refractive index of 2.16–0.01*i* were used for the powder size calculations [17–20]. A SEM image of the starting powders in the milled suspensions is presented in Fig. 1. This sample was prepared by placing a drop of the ball-milled suspension on a glass slide and allowing the ethanol to evaporate. The diameters of the individual particles in the higher magnification image of Fig. 1 agree with the 80 nm size obtained from the particle size analyzer.

YSZ coatings were fabricated from these suspensions at Ames Laboratory (Ames, IA). Suspensions were agitated prior to spraying by a combination of manual mixing and ultrasonic energy. The suspensions were then filtered through a 90 μm sieve while being added to the pressure vessel used to supply the feedstock to the plasma torch. During the SPS process the suspension in this vessel was mixed via a magnetically-driven stir bar to avoid the gravitational separation of YSZ powder from the ethanol solvent reported by Chen et al. [10], Siegert [11], and Oberste Berghaus et al. [16]

The following processing conditions were held constant during all parametric study experiments. The plasma torch was a Praxair (Indianapolis, IN) SG-100 [2] with a 6 mm diameter nozzle. The spray direction of the plasma flow exiting the torch was perpendicular to the substrate, which was a 2.5 cm wide × 10 cm long × 0.5 cm thick copper plate blasted with 24-grit alumina. All suspensions were injected as coherent streams by using nitrogen gas to force the suspension from the pressure vessel through plastic tubing connected to an orifice. The nitrogen gas pressure was adjusted to reach the desired flow velocity of the suspension into the plume. During deposition, the torch rastered horizontally at 29 cm/s across this substrate surface; consecutive passes were separated by 3 mm with an approximate 1 mm overlap. Each coating was comprised of ~20 passes of the torch, and was nominally 30 μm thick. The deposition efficiency was approximately 30%. The backside of the substrate was cooled using two 2.5 cm diameter air jets with a combined volumetric flow rate of roughly 2700 lpm. The velocity of the air exiting each pipe was at least 30 m/s. A steel shroud surrounding the substrate prevented the cooling air from interacting with the depositing YSZ particulates.

Table 1 lists the individual experimental conditions evaluated and the processing parameters varied during this study. (While plasma torch voltage cannot be adjusted directly, it is included in Table 1 to present a more complete overview of the processing conditions.) The first ten rows in Table 1 represent separate spray experiments conducted as part of the parametric study. The last row of Table 1 lists the settings for a spray experiment derived from the process optimization knowledge gained as a result of the parametric study.

The baseline settings listed in the first row were chosen by estimating the optimal conditions suggested from the prior SPS YSZ research cited above. The choice to inject usually through the internal port on the SG-100 was made to increase the dwell time of the YSZ

[2] SG-100 was onfigured with a 3083-129 cathode, 3083-175 anode, and 3083-113 gas injector.

in the plasma. Providing the suspension stream a direct line of sight to the plasma through this port required injecting normal to the spray direction. Consequently, although SPS literature [10,12] indicates better entrainment when the suspension stream is injected at an acute angle relative to the spray direction, the benefits of a longer dwell were thought to outweigh the improved entrainment possible with an acute angle injection. However, for the external injection experiment, the suspension was injected at a 75° angle relative to the spray direction based upon the optimal findings reported in [10]. Additionally, the external injection setup necessitated switching from a 230 μm diameter ruby orifice to a 200 μm diameter stainless steel orifice, which were purchased from Bird Precision (Waltham, MA) and Spray Systems Co. (Wheaton, IL), respectively. Although the orifice diameter was changed for the external injection case, a 20 m/s suspension injection velocity was still used because the suspension appeared adequately entrained in the plume.

2.3. SEM and stereology analysis

The area fractions of unmelted powder and spherical particulates were determined from stereological analyses of the top surface of coatings corresponding to each of the experimental conditions listed in Table 1. For each coating an approximately 5 mm by 5 mm region located at the center of the length and width of the coating was examined. SEM imaging was performed with a Hitachi S-4800 FESEM on gold coated samples. Digital SEM images were recorded at a minimum of six locations within the 25 mm^2 region to provide a roughly uniform sampling of this section of coating top surface. These images were recorded at 10 kX and 15 kX magnifications, corresponding to image areas of ~100 μm^2 and ~50 μm^2, respectively.

During stereological analysis, unmelted powders and spherical-shaped particulates were differentiated based upon feature size and surface morphology. While the overall feature size of unmelted powder agglomerations is microns, closer inspection of the feature will reveal nanometer-sized powders identical in morphology to the starting powder observed in Fig. 1. Spherical particulates are also generally micron-sized because they represent the partial melting or resolidification of many hundreds or thousands of starting powders in the original fragmented droplet, but higher magnification investigations of the particulates reveal a smooth surface. Desirable lamellae, representing coalesced melted powders that strike the substrate in the molten state and spread, were also observed.

The area measurements for stereological analyses were performed on the SEM images for each processing condition using the Scion Image software (Scion Corp. Frederick, MD). The regions of unmelted powder were delineated by hand on the images, and the software measured the areas. Starting with the original micrograph, this process was repeated to measure the total image area covered by spherical objects representing the YSZ that deposited as solid or semi-solid spherical particulates. Due to the coating surface relief, an image could contain regions that lacked the focus or brightness necessary to identify microstructural features. These unusable regions were removed from the images so the total area in them could be measured separately from the areas containing the powder or spherical particulates. The stereological measurements were then used to calculate the area fraction of unmelted powder (f_p) and spherical particulates (f_s) in the micrograph by dividing the total area for each type of microstructural feature by the total usable image area. Note that the surface area fraction data are assumed to be indicative of the microstructural feature volume fractions within the coatings produced by each experimental condition [21].

The powder area fractions determined from coatings belonging to the same experimental condition listed in Table 1 were evaluated using the Ryan–Joiner test to ensure the data set was normal to a significance level of 0.01 [22]. The same test was also used to enforce the normality of the spherical particulate area fraction data sets. To pass these tests, not all area fraction measurements within a set were necessarily included in the data used to establish the average values for an experimental condition. However, each unmelted powder and spherical particulate area fraction data set that passed the normality test was required to be composed of measurements totaling a minimum evaluation area of 500 μm^2 on the coating surface. Additionally, if all the data in a set came from a single coating, the measurements had to be from micrographs providing a roughly uniform sampling of the 5×5 mm examination region.

3. Results and discussion

The average f_p and f_s values observed on the surfaces of coatings produced during the parametric study are shown in Fig. 2. The uncertainty limits of each average bar define an interval about the mean that captures 95% of the t-distribution describing the data used to calculate the average value.

Within the parametric study, the experimental conditions ranked from the lowest to highest f_p content were as follows: baseline, 6 cm standoff |external injection, 10 wt.% powder loading|15 m/s injection velocity, 2 wt.% powder loading, high enthalpy plasma, 4 cm standoff| 23 m/s injection velocity, low enthalpy plasma. (The separation of experimental conditions by a vertical slash indicates that the uncertainty intervals about these area fraction averages exhibit a complete or nearly complete separation.) The order of increasing f_s among the parametric study conditions was as follows: 23 m/s injection|high enthalpy, 4 cm standoff, baseline, external injection, 2 wt.% powder loading, low enthalpy|10 wt.% powder loading, 6 cm standoff, 15 m/s injection velocity. An examination of Fig. 2 also shows that the optimized processing parameters yielded coatings with the smallest f_p and f_s values.

3.1. Guide to analyzing deposition differences

Fragmentation characteristics of the coherent suspension stream have been observed using laser imaging of a stream injected into a plasma produced using parameters similar to the baseline condition listed in Table 1 [23,24]. For the baseline parameters used in this study, the plasma speed in the 7.5 mm diameter anode throat would have been ~1500 m/s [9]. From the calculations of fragmentation time in Ref. [23], the catastrophic suspension stream breakup caused by the baseline plasma settings is expected to have occurred entirely within the 8.5 mm section of the anode throat downstream of the internal injection location. Calculations of the boundary layer thickness in which friction from the anode wall slowed the plasma below 1500 m/s velocity showed this region to be an insignificant fraction of the 7.5 mm anode throat diameter [25], so the plasma in the throat was assumed to have an almost uniform velocity profile.

The diameter and thickness of lamellae in SPS coatings were measured on SEM micrographs showing top surfaces and fractured cross sections. For the baseline condition, the average lamella diameter and thickness were found to be ~3 μm and ~300 nm, respectively, implying an average impacting particulate size of ~1.6 μm diameter [7]. For a 5 wt.% YSZ-loaded suspension, the critical suspension fragment (i.e. ethanol and YSZ powders) would average 8.4 μm in diameter in order to contain the powder mass required for a 1.6 μm diameter YSZ particulate. It is unlikely that this critically-sized fragment would have the momentum required to penetrate further into the plasma than the radius at which it is formed. When comparing deposition differences among the experimental conditions below, suspension fragmentation was considered to be the primary factor affecting the fragment/YSZ path in the plasma; path influences from the plasma swirl, thermophoretic effects, and eddies along the plume periphery as it mixed with the ambient atmosphere were neglected.

Employing the above assumptions, Fig. 3 was developed to provide a framework for discussing the processing parameters effects

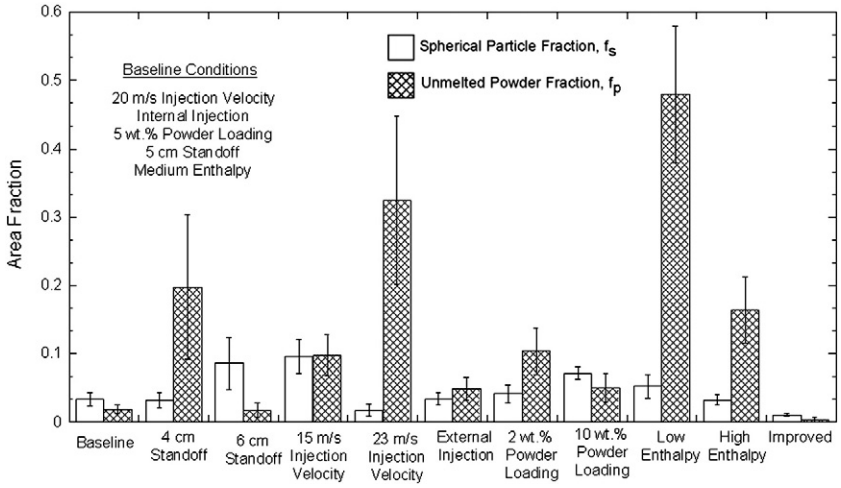

Fig. 2. A bar chart displaying unmelted powder (f_p) and spherical particulate (f_s) area fraction data determined from stereological analyses on each coating sprayed using parameters listed in Table **1**. The error bars define an uncertainty interval about the mean that captures 95% of the t-distribution describing each data set.

on the f_s and f_p area fractions observed on a coating surface. This figure is qualitative, is meant only to illustrate relative differences in SPS experimental conditions, and neglects the flow near the substrate. Given these simplifications, Fig. 3 shows the qualitative shape of zones in which the physical state of a YSZ powder cluster can be expected to change as it moves through the plasma. The difference between the liquidus and solidus temperatures of the ZrO_2–8 wt.% Y_2O_3 is approximately 50 °C [26]. Given the large temperature gradient in the plume, Fig. 3 is simplified to show a single temperature contour combining those isotherms. Plasma in the region to the left of the liquidus/solidus isotherm would exhibit temperatures above the YSZ melting point, and that to right would have temperatures below. The parabolic shape of the liquidus/solidus isotherm depicted in Fig. 3 is in agreement with measured plasma spray plume temperatures [27].

The shapes of the zones in Fig. 3 are based on the heat transfer that YSZ would experience along axial paths at different radial positions in the plasma. The plasma temperature and velocity decrease with increasing radius. As a result, compared to YSZ moving along the centerline, YSZ traveling along Path A in Fig. 3 will move further downstream before melting begins, as reflected by the curvature of the border between the unmelted powder and partially melted zones. Likewise, the zone in which the YSZ is completely melted exhibits a similarly curved nose that terminates at the liquidus/solidus temperature isotherm. After passing the liquidus/solidus temperature isotherm, the partially melted particulates and the molten particulates can begin to re-solidify. The time for molten particulates to cool to the liquidus temperature results in completely molten particulates existing within a portion of the re-solidification zone. Therefore, particulates within the large dashed boundary inside the re-solidification zone of Fig. 3 are considered to be completely molten, while those outside of this envelope are partially melted particulates. It should be noted that the exact position of the regions in Fig. 3 (except the YSZ melting temperature) is different for different particulate diameters.

As mentioned earlier, the suspension was injected radially into the plasma flow for this study. Thus, the suspension stream fragments into droplets over a range of radial locations [23,24]. The variation in fragmentation position along with differences in droplet size can cause YSZ to deposit on the substrate as unmelted powder, spherical particulates, or molten particulates. Unmelted powders depositing on the substrate appear in the coating microstructure as micron-sized clusters comprised of nanometer-sized powders. The spherical particulates are distinguishable from the powder clusters because the former exhibit a smooth, uniform surface. The molten particulates impacting the substrate become the lamellae within the coating microstructure.

3.2. Analysis of deposition differences

3.2.1. Effect of stand off distance

Fig. 2 shows that the fraction of spherical particulates (f_s) appearing in the coating was not affected by increasing the standoff distance from 4 to 5 cm, while a 6 cm standoff produced a significant increase

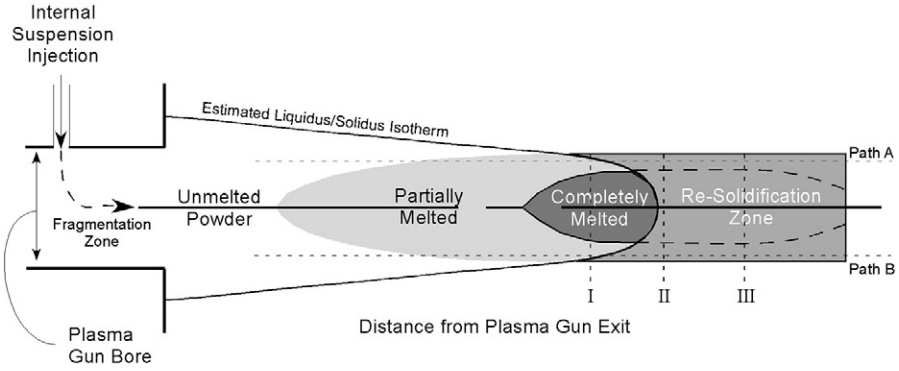

Fig. 3. Qualitative illustration showing how heat transfer within the plasma can change the YSZ physical state from unmelted powder (white) to partially melted particulate (lightest gray) to completely melted particulate (darkest gray) to re-solidified spherical particulate (medium gray). The dashed arrow represents the ideal radial penetration of a suspension fragment into the plasma. Paths A and B correspond to non-optimized entrainment of a fragmented droplet in the plume.

in f_s. This result is also demonstrated in the micrographs of Fig. 4a–c. This trend in the f_s data suggests that substrates at 4 cm and 5 cm from the torch exit were close enough to the liquidus isotherm that the deposition of liquid YSZ particulates did not vary appreciably between these locations (sketched as positions I and II in Fig. 3). Conversely, between 5 and 6 cm from the torch exit, the plasma likely cooled to the point that significantly more molten particulates began to re-solidify prior to striking the substrate. This result is illustrated in Fig. 3 by the relative axial positions II and III within the re-solidification region.

Based upon the YSZ conditions shown in Fig. 3, the coatings with different standoff distances should display no differences in the f_p amounts. This expectation is confirmed in the results of the baseline (5 cm) and 6 cm standoff coatings, but the f_p data in Figs. 2 and 4 show an increase at the 4 cm standoff. The larger fraction of unmelted powder in the 4 cm standoff coating is most likely the byproduct of a suspension injection nozzle obstruction, which caused this particular experiment to be stopped halfway through the planned coating process. Injection nozzle obstructions reduced the suspension stream velocity significantly, which decreased the penetration of the stream into the plasma and produced observable changes in the plume brightness. With fewer droplets penetrating to the center of the plume, the YSZ gained less heat and produced more coating defects; these effects are more fully discussed in Section 3.2.2.

3.2.2. Effect of suspension injection velocity

For a given injection orifice diameter, varying the suspension stream injection velocity has two effects on the stream-plasma interactions. The penetration of the liquid stream into the plasma increases with injection velocity [24], as does the power required to vaporize the liquid and melt the YSZ. Using thermophysical data from Ref. [11,28] and the NIST Chemistry WebBook [29], Fig. 5 illustrates this power requirement change with injection velocity for the present experimental setup. From Fig. 5, a 5 wt.% YSZ suspension injected at 15 m/s, 20 m/s, and 23 m/s respectively requires 750 W, 975 W, and 1200 W of power to vaporize all of the ethanol and to heat and to melt all of the YSZ.

Figs. 2 and 4d show that the 15 m/s injection velocity condition led to higher f_s and f_p values than the baseline case (20 m/s). The radial temperature profile of the plume can vary by several hundred Kelvin per millimeter, meaning the enthalpy available for melting YSZ exhibits a similar rate of decrease from the core to the fringes of the plasma plume [23,27]. Therefore, it is not surprising that the

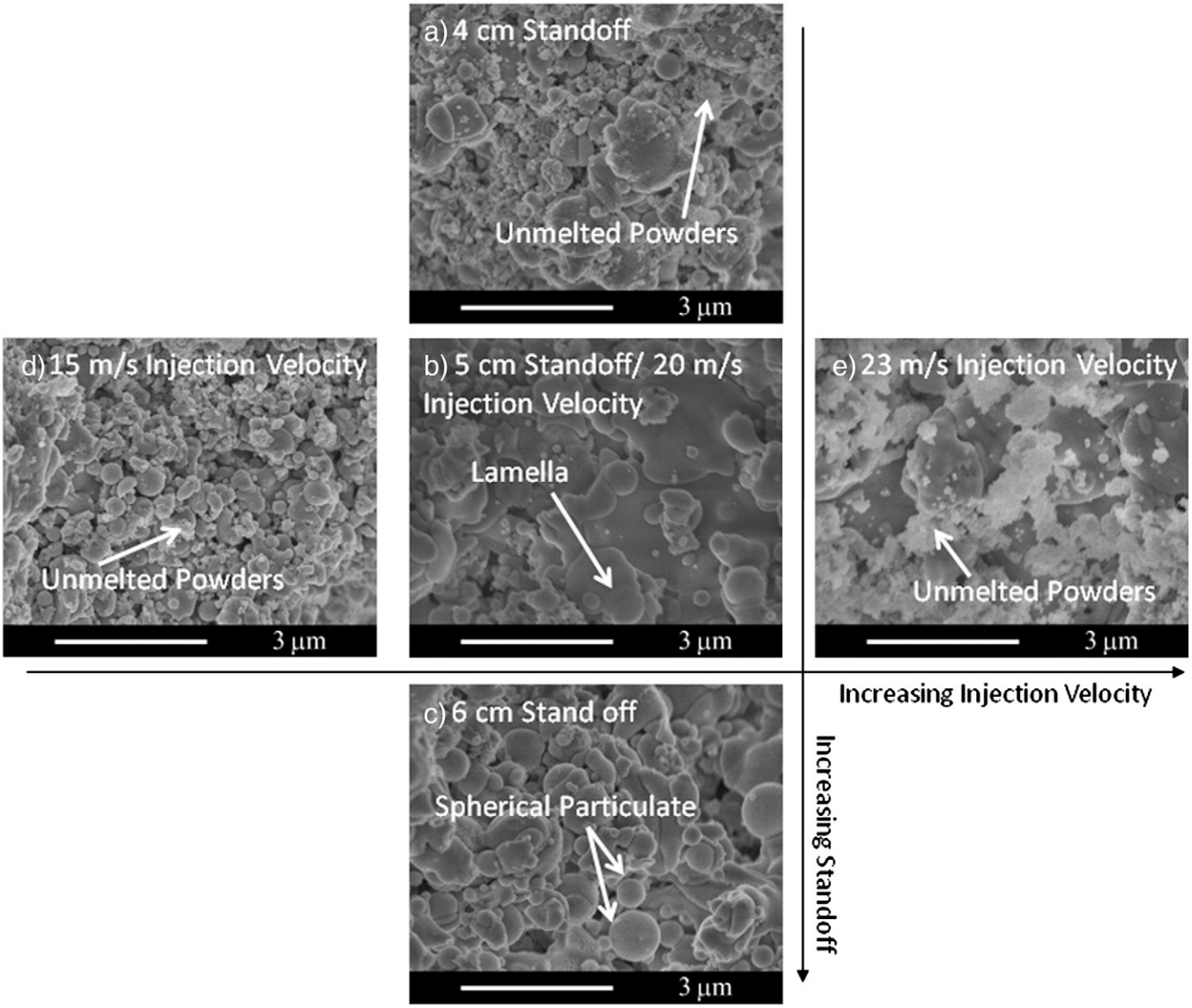

Fig. 4. SEM images showing the microstructural features on the top surfaces of the coatings fabricated with the (a) 4 cm standoff, (b) 5 cm standoff and 20 m/s injection velocity (baseline), (c) 6 cm standoff, (d) 15 m/s injection velocity, and (e) 23 m/s injection velocity processing conditions.

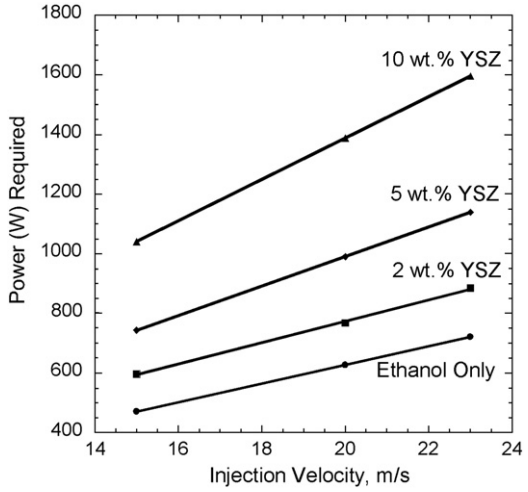

Fig. 5. Plot of the power required to vaporize ethanol and heat the YSZ powders to melting as a function of injection velocity and powder loading.

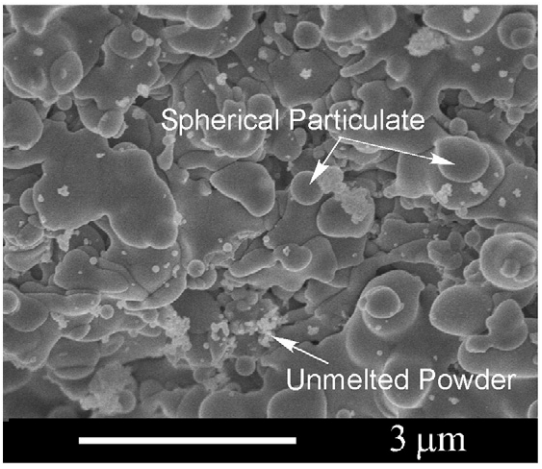

Fig. 6. SEM image showing the microstructural features on the top surface of a coating fabricated using the external injection setup.

25% decrease in injection velocity produced three times more spherical particulates and unmelted powder than the baseline, despite the 15 m/s injection velocity condition requiring ~20% less power to melt completely the injected YSZ. With the shorter penetration into the plasma, less powder was melted, and more of the melted powder began to resolidify before deposition (to see this effect, compare Path A to the centerline in Fig. 3).

Fig. 2 also shows that the fraction of unmelted powder (f_p) for the 23 m/s injection velocity condition (see Fig. 4e) is an order of magnitude higher than that of the baseline coating, which does not follow from the reasoning above. However, a rivulet of the suspension was observed to form below the torch nozzle exit during this experiment. For this situation to occur, some of the injected suspension had to pass completely through the plasma, collect on the anode throat bottom, and be dragged out of the torch by the plasma flow. This condition increased the concentration of suspension fragments within in the cooler fringe of the plasma plume, leading to more deposition of unmelted powder, yet the fraction of spherical particulates for the 23 m/s injection velocity case was about one-half that of the baseline. While a higher injection velocity increases the volumetric flow of suspension into the plasma, the fact that a significant amount of suspension passed through the plasma with a 23 m/s injection velocity is likely to mean more enthalpy was available per fragment in the plasma core than under baseline conditions. This scenario is the equivalent of moving the melting temperature isotherm in Fig. 3 downstream, which would produce a larger change in width of the completely melted region than in the partially melted region. Additionally, the decrease in f_s may have been influenced by the deeper stream penetration increasing the fragments entrained near the plume centerline.

3.2.3. Effect of injection location

When the injection location was changed to external to the torch, the f_p approximately doubled compared to the baseline, while the f_s saw no statistically significant change. The former result, seen in micrographs in Figs. 4b and 6, can be connected to differences in the fragmentation behavior between these experiments. Outside the torch, the plume spreads out and has a plasma velocity field with a larger radius than the torch nozzle [30]. With the external injection setup, the suspension stream was affected by this larger, but slower, plume at greater distances from the plasma centerline than for the internal injection conditions. As a result, the suspension stream fragmentation in the external injection case initiated at a larger radius than the wall of the anode throat; this behavior is suggested by high speed imaging of an externally-injected suspension stream (e.g., Fig. 3 in Ref. [23]). A small fraction of the suspension is then carried off in the cooler fringes of the expanding plume, where the enthalpy is insufficient to melt the YSZ fully, thus increasing the fraction of unmelted powder in the coating. The rest of the stream penetrates the plume much the same as the internal injection case, except the effective standoff distance is less in the external case. Noting that the baseline (5 cm standoff) and the 4 cm case have approximately the same f_s, it is not surprising that the external injection case does not see an increase in f_s.

3.2.4. Effect of suspension powder content

Changes in suspension powder loading can have different effects on the sprayed coatings. One effect is the change in the total enthalpy needed to melt the solid. Fig. 5 shows the power required to vaporize all of the ethanol and to heat and melt all of the YSZ injected as a function of injection velocity and solid loading. For the baseline processing conditions, ~1000 W is required to vaporize the ethanol and heat and melt the YSZ powders. This power represents 2.6% of the total power provided (38 kW) to the plasma gun. The total enthalpy that is in the plume has been reported as ~1/3 of the total provided energy [31], so these changes in solid loading should have little effect on the position of the melting isotherm.

A prior SPS study has demonstrated that a stream of ethanol fragments sooner than an ethanol–zirconia suspension stream containing 7 wt.% powder [23]. Therefore, differences in the radial penetration before the onset of fragmentation between the 2, 5, and 10 wt.% powder streams were expected to contribute to the f_p and f_s differences between the coatings produced with these suspension formulations. Earlier fragmentation and the corresponding movement of the YSZ through a cooler region of the plume is thought to be the reason the 2 wt.% loading f_p in Fig. 2 is roughly five times larger than the baseline, a finding illustrated in Fig. 7a–b. From the results in Section 3.2.2, one might expect the lower penetration to give a higher f_s value than the baseline, as with the 15 m/s injection velocity case. However, due to the lower powder content, the ratio of plume enthalpy to the total enthalpy required for evaporating solvent and melting YSZ is larger for the 2 wt.% case than for the baseline, so more enthalpy is available to melt the ceramic in the former. On the other hand, the lower YSZ loading in similarly sized suspension droplets means the YSZ particulates are smaller than the baseline and resolidify faster. A quantification of these tradeoffs is impossible without knowledge of the droplet size distributions and fragmentation radii, but the result in these experiments is a statistically small increase in f_s at 2 wt.% solid loading.

The radial position of fragmentation for the 10 wt.% case should have been deeper than the baseline, yet the f_p for this condition was ~2.5 times the baseline value. The primary cause for this increase

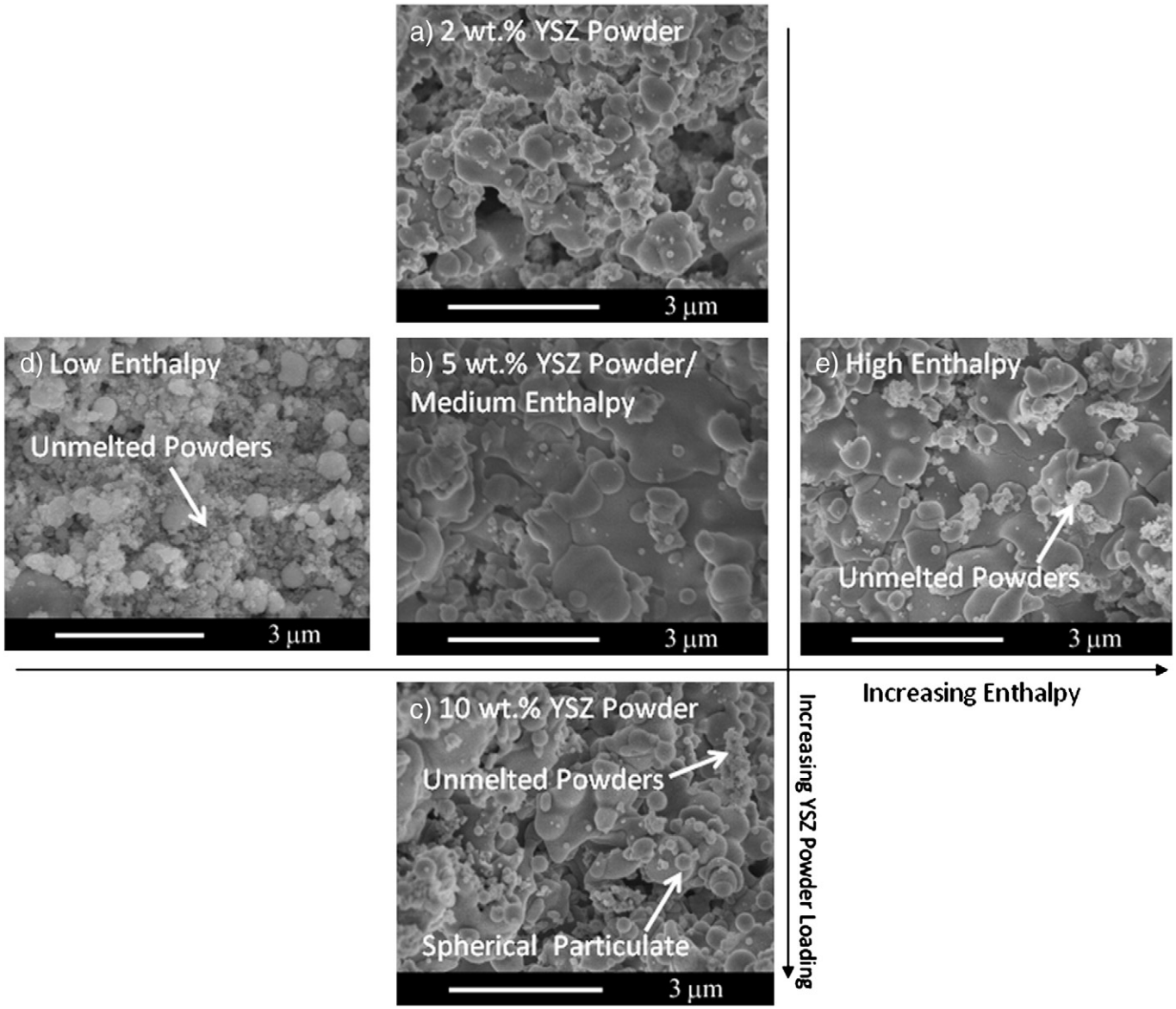

Fig. 7. SEM images showing the microstructural features on the top surfaces of the coatings fabricated with the (a) 2 wt.% powder loading, (b) 5 wt.% powder loading and medium enthalpy (baseline), (c) 10 wt.% powder loading, (d) low plasma enthalpy, and (e) high plasma enthalpy processing conditions.

is attributed to the increased size of the agglomerated powder masses which contain twice as much powder and, thus, take longer to melt completely. This hypothesis is supported by observation of larger powder regions in the 10 wt.% loading coating (Fig. 7c vs. b). Similarly, the 10 wt.% loading f_s was approximately double the baseline value. This result indicates that any penetration improvements achieved by increasing the powder loading were offset by the decrease in the completely melted zone width brought on by the larger YSZ powder agglomerates.

3.2.5. Effect of plasma enthalpy

The plasma enthalpy was controlled by adjusting the electrical current and the composition and flow rates of the plasma-forming gasses, as listed in Table 1, producing torch powers of 21 kW, 38 kW (baseline), and 42 kW. Lowering the plasma enthalpy decreases the overall temperature of the plasma. This change will move the axial position of the noses on both the partially and completely melted zones farther from the torch exit and the liquidus/solidus isotherm closer to the torch exit. As a result, the lengths and widths of the partially and completely melted zones contract, and the areas of the unmelted powder zones increase.

The 300 A decrease in the torch current when switching from the baseline to the low enthalpy condition also lowers the average plasma velocity in the torch by several hundred meters per second below the ~1500 m/s speed discussed in Section 3.1 [9]. This decrease would tend to increase the stream penetration before fragmentation and the average droplet size. Based upon the stereological analyses, the smaller completely melted zone in the plume produced at the lower enthalpy and the larger droplets more than compensated for the increased penetration; the low-enthalpy condition f_p value in Fig. 2 is twenty-four times the baseline value, a result which is also reflected in the microstructures in Fig. 7b and d. The low enthalpy f_s value was also larger than that for the baseline, but the disparity in this case was only a factor of 1.5.

The plasma conditions detailed above should have been reversed with the high enthalpy settings, yet the f_p and f_s results relative to the baseline were not the opposite of those from the low enthalpy case. The f_p value for the high enthalpy condition is also higher than the baseline results. Higher power conditions can be connected to an increased

plasma velocity in the torch [9], which decreases the penetration of fragmented droplets into the plasma core and the mean size of the droplets. Consequently, more droplets travel to the substrate within the cooler plume periphery comprising the unmelted powder zone. Similarly, more droplets would also be expected to travel along radial positions that, for the baseline conditions, would have yielded spherical particulates in the coating. However, the f_s values for the baseline and high enthalpy conditions are equivalent (Fig. 5b and e). This outcome can be explained by the plasma temperature increase and smaller YSZ agglomerate size in the high enthalpy case leading to an expansion of the completely melted region.

3.3. Final process modifications

The parametric study findings presented currently and the plasma-spray literature were employed to further improve the SPS experimental setup to produce coatings that minimized f_s and f_p. External suspension injection was abandoned in favor of the internal injection setup due to the reduction in f_p observed with the latter. The standard suspension powder loading was increased from 5 to 8 wt.% to reduce the spray time required to make a coating by increasing the amount of YSZ depositing. To promote the deposition of this YSZ in the molten state, the plasma-forming gas mixture was changed to increase the plasma enthalpy. Based upon DC plasma torch literature, a 25 vol.% Ar–75 vol.% He gas composition was selected. [32] Different flow rates of 25/75 vol.% Ar–He gas mixtures were evaluated at a torch current of 1000 A to determine which one maximized the torch voltage, and thus, the plasma temperature [8]. (The torch current was capped at 1000 A to reduce electrode wear.) The highest voltage obtained during this empirical investigation was 50 V, which corresponded to a total gas flow rate of 80 slm and a torch power of 50 kW.

The above processing changes necessitated re-evaluating the suspension injection velocity. However, rather than optimizing this parameter from coating examinations, a viewing port was utilized to monitor the torch exit during spraying. If ceramic was observed to be collecting near the torch exit bottom, the injection velocity was reduced by reducing the nitrogen gas pressure; conversely, the injection velocity was increased if ceramic began collecting along the top of the torch exit. Adjusting the injection pressure to the unique conditions of an experiment resulted in multiple injection velocities being used, but 21 m/s was the average injection velocity for experiments involving 8 wt.% powder suspensions and a 20 slm Ar–60 slm He gas mixture interacting with a 50 kW electric arc.

The complete set of improved spray parameters is listed in Table 1, and an example of the coating microstructure resulting from these settings is shown in Fig. 8. The average f_p and f_s data from stereological analyses performed on coatings fabricated with the improved parameters are plotted in Fig. 2. This figure shows that these averages are significantly lower than any of the values from other experimental conditions.

4. Summary

In summary, a parametric study was conducted to determine the effects on the final coating microstructure of the following suspension plasma spray processing parameters: torch standoff, suspension injection velocity, injector location, powder loading in the suspension, and plasma enthalpy. Of particular interest in this study was the presence of two undesirable microstructural features: (1) unmelted powders, which appeared as micron-sized clusters of the 80 nm diameter YSZ feedstock particles, and (2) spherical particulates, which resulted from partial melting or re-solidification of the feedstock YSZ prior to deposition.

The largest percentage (~50%) of coating surface area covered with unmelted powder resulted from the experimental condition yielding the lowest plasma enthalpy. The area fraction of unmelted powder was also found to increase for conditions that increased the fragmentation of the suspension in the colder fringes of the plume. This non-optimal stream fragmentation occurred when the suspension injection velocity was either too low or too high, as the plasma velocity increased, and as the suspension powder loading decreased. The highest percentage of coating surface area covered with unmelted powder as a result of non-optimal fragmentation was 33%.

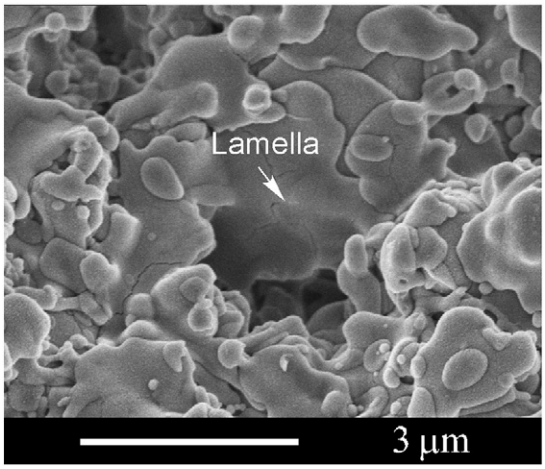

Fig. 8. SEM images showing the microstructural features on the top surface of a coating produced from the improved processing parameters listed in Table 1.

The largest area fractions of spherical particulates (f_s) resulted from the 15 m/s suspension injection velocity condition (f_s~0.1) and from the 6 cm standoff condition (f_s~0.09). The 15 m/s injection velocity was believed to lead to an earlier onset of stream fragmentation in a colder region of the plasma, which increased the amount of partially-melted YSZ particulates. The longer standoff distance experiment allowed more time for the re-solidification of molten YSZ particulates prior to substrate impact.

In this study, the optimum deposition occurred when using a 5 cm standoff and a suspension containing 8 wt.% YSZ powder that was injected at 21 m/s (~50 ml/min) through the torch body into plasma produced from a 20 slm Ar–60 slm He gas mixture ionized by a 50 kW arc. The coatings produced with these processing parameters still contained undesired spherical particulates and unmelted powder, but the combination of these features comprised less than 2% of the area on the coating top surface.

Acknowledgments

Major portions of this research were funded by the National Science Foundation via grant CMMI-0456534. Dr. Daniel Sordelet and Matthew Besser of Ames National Laboratory facilitated coating fabrication. Ames Laboratory is operated for the U.S. Department of Energy by Iowa State University under Contract No. DE-AC02-07CH11358.

References

[1] R.A. Miller, J. Therm. Spray Technol. 6 (1) (1997) 35.
[2] U. Schulz, C. Leyens, K. Fritscher, M. Peters, B. Saruhan-Brings, O. Lavigne, J.-M. Dorvaux, M. Poulain, R. Mévrel, M. Caliez, Aerosp. Sci. Technol. 7 (2003) 73.
[3] R. McPherson, Surf. Coat. Technol. 39/40 (1989) 173.
[4] US Patent # 2006/0222777 A1, Method for Applying a Plasma Sprayed Coating using Liquid Injection, A.J. Skoog, J.A. Murphy, T.J. Tomlinson.
[5] P. Fauchais, V. Rat, J.-F. Coudert, R. Etchart-Salas, G. Montavon, Surf. Coat. Technol. 202 (2008) 4309.
[6] F. Tarasi, M. Medraj, A. Dolatabadi, J. Oberste-Berghaus, C. Moreau, J. Therm. Spray Technol. 17 (5–6) (2008) 685.
[7] K. VanEvery, M.J.M. Krane, R.W. Trice, Column Formation in Suspension Plasma-Sprayed Coatings and Resultant Properties, J. Therm. Spray Techn. 20 (4) (2011) 817.
[8] P. Fauchais, J. Phys. D: Appl. Phys. 37 (2004) R86.

[9] M.P. Planche, J.F. Coudert, P. Fauchais, Plasma Chem. Plasma Process. 18 (2) (1998) 263.
[10] J. Oberste Berghaus, S. Bouaricha, J.-G. Legoux, C. Moreau, in: C. Berndt, E. Lugsheider (Eds.), Proceedings of the International Thermal Spray Conference, ASM International, Basel, Switzerland, 2005, May 2-4, 2005.
[11] Z. Chen, R.W. Trice, M. Besser, X. Yang, D. Sordelet, J. Mater. Sci. 39 (2004) 4171.
[12] R. Siegert, A Novel Process for the Liquid Feedstock Plasma Spray of Ceramic Coatings with Nanostructural Features, Doctoral Thesis, Institut fur Werkstoffe und Verfahren der Energietechnik, 2005.
[13] H. Kassner, Proceedings of the 32nd International Conference on Advanced Ceramics and Composites, 2008, Daytona Beach (Florida), USA.
[14] C. Delbos, J. Fazilleau, V. Rat, J.F. Coudert, P. Fauchais, L. Bianchi, in: C. Berndt, E. Lugsheider (Eds.), Proceedings of the International Thermal Spray Conference, ASM International, Basel, Switzerland, 2005, May 2–4, 2005.
[15] R. Siegert, J.-E. Doring, J.-L. Marques, R. Vassen, D. Sebold, D. Stover, in: C. Berndt, E. Lugsheider (Eds.), Proceedings of the International Thermal Spray Conference, ASM International, Basel, Switzerland, 2005, May 2–4, 2005.
[16] J. Oberste Berghaus, S. Bouaricha, J.-G. Legoux, C. Moreau, T. Chraska, in: C. Berndt, E. Lugsheider (Eds.), Proceedings of the International Thermal Spray Conference, ASM International, Basel, Switzerland, 2005, May 2–4, 2005.
[17] Coulter® LS Series Product Manual, Coulter Corporation, Miami, 1994 c.
[18] A. Jillavenkatesa, S.J. Dapkunas, L.-S.H. Lum, NIST Special Publication 960–1: Particle Size Characterization, http://www.msel.nist.gov/practiceguides/SP960_1.pdf2001.
[19] S. Raghavan, H. Wang, R.B. Dinwiddie, W.D. Porter, M.J. Mayo, Scr. Mater. 39 (8) (1998) 1119.
[20] J.R. Piascik, J.Y. Thompson, C.A. Bower, B.R. Stoner, J. Vac. Sci. Technol., A 23 (5) (2005) 1419.
[21] K.J. Kurzydlowski, B. Ralph, The quantitative description of the microstructure of materials, CRC Press, New York, 1995 c.
[22] J.L. Devore, Probability and Statistics for Engineering and the Sciences, 5th Ed. Brooks/Cole, Pacific Grove, CA, 2000 c.
[23] J. Fazilleau, C. Delbos, V. Rat, J.F. Coudert, P. Fauchais, B. Pateyron, Plasma Chem. Plasma Process. 26 (2006) 371.
[24] P. Fauchais, R. Etchart-Salas, V. Rat, J.F. Coudert, N. Caron, K. Wittmann-Teneze, J. Therm. Spray Technol. 17 (1) (2008) 31.
[25] F.P. Incropera, D.P. DeWitt, 5th Edition, John Wiley & Sons, Inc, New York, 2002, p. 924, c.
[26] H.G. Scott, J. Mater. Sci. 10 (1975) 1527.
[27] J.R. Fincke, W.D. Swank, D.C. Haggard, Plasma Chem. Plasma Process. 13 (4) (1993) 579.
[28] W.D. Porter, Oak Ridge National Laboratory, differential scanning calorimetry data for ZrO_2–8 wt% Y_2O_3 made available to the authors, 2006.
[29] http://webbook.nist.gov/chemistry.
[30] J.R. Finke, D.M. Crawford, S.C. Snyder, W.D. Swank, D.C. Haggard, R.L. Williamson, Int. J. Heat Mass Transfer 46 (2003) 4201.
[31] J. M. Houben, Relations of the Adhesion of Plasma-Sprayed Coatings to the Process Parameters Size, Velocity and Heat Content of the Spray Particles. Ph.D. Thesis, Technical University Eindhoven, The Netherlands (1998).
[32] V. Rat, J.F. Coudert, J. Phys. D: Appl. Phys. 39 (2006) 4799.